Carcinogenesis vol.31 no.10 pp.1889–1896, 2010
doi:10.1093/carcin/bgq153
Advance Access publication July 26, 2010

Loss of p15/Ink4b accompanies tumorigenesis triggered by complex DNA double-strand breaks

Cristel V.Camacho[1], Bipasha Mukherjee[1], Brian McEllin[1], Liang-Hao Ding[1], Burong Hu[2,3], Amyn A.Habib[4,5], Xian-Jin Xie[6], Chaitanya S.Nirodi[1], Debabrata Saha[1], Michael D.Story[1], Adayabalam S.Balajee[2], Robert M.Bachoo[4], David A.Boothman[1,6,7] and Sandeep Burma[1,*]

[1]Department of Radiation Oncology, University of Texas Southwestern Medical Center at Dallas, Dallas, TX 75390, USA, [2]Department of Radiation Oncology, Center for Radiological Research, Columbia University, New York, NY 10032, USA, [3]Key Laboratory of Heavy Ion Radiation Biology and Medicine, Institute of Modern Physics, Chinese Academy of Sciences, Lanzhou, People's Republic of China, [4]Department of Neurology, University of Texas Southwestern Medical Center at Dallas, Dallas, TX 75390, USA, [5]Department of Neurology, North Texas VA Medical Center, Dallas, TX 75216, USA and, [6]Simmons Comprehensive Cancer Center and [7]Department of Pharmacology, University of Texas Southwestern Medical Center at Dallas, Dallas, TX 75390, USA

*To whom correspondence should be addressed. Division of Molecular Radiation Biology, Department of Radiation Oncology, University of Texas Southwestern Medical Center, 2201 Inwood Road, NC7.214E, Dallas, TX 75390, USA. Tel: +1 214 648 7440; Fax: +1 214 648 5995; Email: sandeep.burma@utsouthwestern.edu

DNA double-strand breaks (DSBs) are the most deleterious lesion inflicted by ionizing radiation. Although DSBs are potentially carcinogenic, it is not clear whether complex DSBs that are refractory to repair are more potently tumorigenic compared with simple breaks that can be rapidly repaired, correctly or incorrectly, by mammalian cells. We previously demonstrated that complex DSBs induced by high-linear energy transfer (LET) Fe ions are repaired slowly and incompletely, whereas those induced by low-LET gamma rays are repaired efficiently by mammalian cells. To determine whether Fe-induced DSBs are more potently tumorigenic than gamma ray-induced breaks, we irradiated 'sensitized' murine astrocytes that were deficient in Ink4a and Arf tumor suppressors and injected the surviving cells subcutaneously into nude mice. Using this model system, we find that Fe ions are potently tumorigenic, generating tumors with significantly higher frequency and shorter latency compared with tumors generated by gamma rays. Tumor formation by Fe-irradiated cells is accompanied by rampant genomic instability and multiple genomic changes, the most interesting of which is loss of the p15/Ink4b tumor suppressor due to deletion of a chromosomal region harboring the *CDKN2A* and *CDKN2B* loci. The additional loss of p15/Ink4b in tumors derived from cells that are already deficient in p16/Ink4a bolsters the hypothesis that p15 plays an important role in tumor suppression, especially in the absence of p16. Indeed, we find that reexpression of p15 in tumor-derived cells significantly attenuates the tumorigenic potential of these cells, indicating that p15 loss may be a critical event in tumorigenesis triggered by complex DSBs.

Introduction

Ionizing radiation (IR) has long been recognized as a carcinogen, although the exact mechanisms underlying radiation-induced carcinogenesis remain largely unknown (1,2). The carcinogenic effects of radiation are attributed to its clastogenic and mutagenic effects, although unique radiation-induced genetic alterations have yet to be identified in humans except in the case of thyroid cancers (3,4). The most deleterious lesion inflicted by IR is the DNA double-strand break (DSB). A causal relationship between DSBs and cancer is clear from the cancer predisposition of humans (and knockout mice) with deficiencies in proteins responding to DSBs (5). Although DNA breaks can be potentially carcinogenic, it is not clear whether complex DSBs that are refractory to repair are more potently tumorigenic than simple breaks that can be rapidly repaired, correctly or incorrectly, by mammalian cells.

Although DSBs induced by gamma rays (i.e. low-linear energy transfer [LET] radiation) are amenable to repair, the same does not necessarily hold true for damage induced by high atomic number and energy (HZE) particles (i.e. high-LET radiation) that inflict complex DNA lesions (6). HZE particles are an important component of galactic cosmic rays and are of serious concern to astronauts on long-duration space missions due to their proposed higher carcinogenic potential; however, considerable uncertainties exist regarding the estimation of cancer risks from these particles (7). Importantly, heavy ion beams are being increasingly and effectively used for targeted cancer therapy; therefore, it is critical to understand the potential for induction of secondary cancers from these ions (8,9). We previously demonstrated that DSBs induced by 1 GeV/nucleon Fe ions are slowly and incompletely repaired, triggering persistent DNA damage signaling events and senescence in primary human skin fibroblasts, whereas DSBs induced by gamma rays are rapidly and completely repaired by these cells (10).

To investigate whether complex DNA breaks that are slowly and incompletely repaired are more potently tumorigenic compared with breaks that are efficiently repaired, we used a very simple and sensitive paradigm of cellular transformation. We previously demonstrated that primary Ink4a/Arf−/− astrocytes are immortal but not tumorigenic (11). However, these 'sensitized' cells can be potently transformed by a single oncogenic event, such as expression of kRas, myrAkt or EGFRvIII. By assessing the tumor-forming abilities of irradiated Ink4a/Arf−/− astrocytes, we directly investigated the transforming potential of Fe ions compared with gamma rays with the goal of identifying Fe-induced genomic changes responsible for triggering tumorigenesis in this model system. We show here that Fe ions are potently tumorigenic when directed to these sensitized astrocytes, generating tumors with significantly higher frequency and shorter latency compared with tumors generated by gamma rays. Tumor formation by Fe-irradiated cells is accompanied by rampant genomic instability and multiple genomic changes, the most interesting of which is loss of the p15/Ink4b tumor suppressor due to deletion of the chromosomal region harboring the *CDKN2A* and *CDKN2B* loci. The additional loss of p15/Ink4b in tumors derived from p16/Ink4a-null astrocytes is interesting and bolsters the hypothesis that p15 has a critical 'backup' function in p16-mediated tumor suppression (12). Indeed, we find that reexpression of p15/Ink4b in tumor-derived cells delays tumor progression thereby confirming the importance of p15 loss in particle-induced cellular transformation. In sum, this work reports detailed analyses of genomic changes occurring after HZE-particle irradiation that possibly underlie cellular transformation and tumorigenesis. Our data provide a greater understanding of the link between complex DNA damage induced by charged particles and the resultant genomic changes triggering radiation-induced carcinogenesis.

Abbreviations: DSB, double-strand break; HZE, high atomic number and energy; IR, ionizing radiation; LET, linear energy transfer; M-FISH, Multicolor fluorescence *in situ* hybridization; PCR, polymerase chain reaction.

Materials and methods

Cell culture

Primary murine astrocytes were isolated from Ink4a/Arf−/− 5-day-old pups as described (11). Primary mouse astrocytes and *ex vivo* tumor cultures were all

maintained in α-modified Eagle's medium containing 10% fetal bovine serum in a humidified 37°C incubator in the presence of 5% CO_2.

Irradiations

Fe ions with a kinetic energy of 1 GeV/nucleon were provided by the National Aeronautics and Space Administration Space Radiation Laboratory at Brookhaven National Laboratory as described (10). For gamma irradiation, a ^{137}Cs source (JL Shepherd and Associates, San Fernando, CA) was used. For mock irradiations, cells were placed in the gamma- or Fe-irradiation chamber for a comparable period of time.

Colony formation assays

For colony formation assays, 300 cells were plated in triplicate 60 mm dishes, irradiated with graded doses of radiation (high- or low-LET, as indicated) and surviving colonies stained with crystal violet 6–8 days postirradiation as described (10).

Immunofluorescence staining, immunoprecipitations and western blotting

Immunofluorescence staining of cells and tissue sections and western blotting of whole-cell extracts were performed as described (13). Antibodies used were anti-actin (Sigma, St Louis, MO), anti-Ki67 (Novocastra, Wetzlar, Germany), anti-53BP1, anti-phospho-Akt(Ser473), anti-phospho-Erk1/2(Thr202/Tyr204), anti-CDK4, anti-CDK6 (Cell Signaling, Beverly, MA), anti-p15 (Santa Cruz, Santa Cruz, CA), anti-V5, anti-V5-fluorescein isothiocyanate, (Invitrogen, Carlsbad, CA) and rhodamine red-conjugated goat anti-mouse and fluorescein isothiocyanate-conjugated goat anti-rabbit (Molecular Probes, Eugene, OR). Anti-V5 antibody (Invitrogen) and Dynabeads® sheep anti-mouse IgG (Invitrogen) were used for immunoprecipitations.

DSB repair assay

DSB repair rates were assessed by quantifying the time-dependent dissolution of γH2AX and 53BP1 foci as described (10).

Metaphase spreads, Multicolor fluorescence in situ hybridization and telomere fluorescence in situ hybridization

Metaphase chromosome spreads were prepared after treatment with 1 μg/ml colcemid (Sigma) using standard procedures. Multicolor fluorescence *in situ* hybridization (M-FISH) was performed using the 21XMouse M-FISH probe kit according to manufacturer's specifications (MetaSystems, Altlussheim, Germany). For telomere fluorescence *in situ* hybridization, a Cy3-labeled peptide nucleic acid probe was used and hybridization was performed as described (14).

Subcutaneous injections

Cells (as indicated) were suspended in Hank's Buffered Salt Solution and 10^6 cells were subcutaneously injected into the flanks of 6-week-old Nu/Nu nude mice (Charles River Laboratories International, Wilmington, MA). Mice were monitored daily for tumor formation and growth over a span of 8 weeks. All animal studies were performed under protocols approved by the Institutional Animal Care and Use Committee of University of Texas Southwestern Medical Center.

Polymerase chain reaction, quantitative PCR and quantitative reverse transcription–PCR

DNA was isolated using the DNeasy Blood and Tissue Kit (Qiagen, Germantown, MD). RNA was extracted using RNeasy Mini Kit (Qiagen) and complementary DNA synthesized using SuperScriptIII First Strand Synthesis System (Invitrogen). Quantitative polymerase chain reaction (PCR) and quantitative reverse transcription–PCR were carried out using the LightCycler-FastStart DNA Master SYBR-Green I kit (Applied Biosystems, Foster City, CA). Standard curves were established following serial sample dilutions and data normalized to the housekeeping gene glyceraldehyde 3-phosphate dehydrogenase.

Array comparative genomic hybridization

Genomic DNA from two mock-irradiated parental cell cultures and two *ex vivo* tumor cultures were extracted using the DNeasy Blood and Tissue Kit (Qiagen), and after quality check, 2.5 μg of DNA for each sample was sent to the NimbleGen Inc. (Madison, WI) mouse array comparative genomic hybridization service. The NimbleGen MM8 WG CGH array, which spans the entire non-repetitive regions of the mouse genome in a single array, was used. Normalization and segmentation of raw signals were processed by NimbleGen and subsequently loaded into Nexus Copy Number Analysis software (Biodiscovery, El Segundo, CA) for rank segmentation analysis and generation of ratios of DNA copy number changes.

Generation of tumor cells reexpressing p15/Ink4b

Human *p15/Ink4b/CDKN2B* complementary DNA was obtained from Addgene, Cambridge, MA (pCRII-p15; 16454) and sequentially cloned into pLenti6.3/V5-DEST by BP and LR clonase reactions (Invitrogen). The final vector, pLenti6.3/p15-V5/DEST, was confirmed by sequencing. The vector pLenti6.3/V5-GW/*lacZ* (Invitrogen) was used as a control in transfections. pLenti6.3/p15-V5/DEST or pLenti6.3/V5-GW/*lacZ* vectors were transfected into Fe-derived tumor cells using Lipofectamine 2000 (Invitrogen) as per manufacturer's protocol. To establish stable clones, transfected cells were selected with 5 μg/ml blasticidin (Invitrogen) and screened by western blotting with anti-V5 antibody (Invitrogen).

Statistical analyses

Frequencies of tumor formation by Fe- and gamma-irradiated cells were compared using Fisher's exact test. Tumor growth curves for these two irradiation conditions were compared using the generalized estimating equations method with AR(1) correlation structure used. All the statistical analyses were performed with SAS 9.1.3 Service Pack 3.

Results

DSBs induced by Fe ions are refractory to repair

For these studies, we used a very simple and sensitive paradigm of cellular transformation—'sensitized' Ink4a/Arf−/− astrocytes that can be potently transformed by a single oncogenic event (11). We previously reported that DSBs induced in human fibroblasts by 1 GeV/nucleon Fe ions are repaired slowly and incompletely compared with those induced by gamma rays (10). We first confirmed that this difference in DSB repair is also manifested in the primary murine Ink4a/Arf−/− astrocytes used in this study. Fe-irradiated cells exhibited slower DSB repair kinetics, as well as persistent DNA lesions at 24 h. In contrast, gamma-irradiated cells completely repaired their DNA by 8 h (Figure 1A). The higher relative biological effectiveness of Fe ions compared with gamma rays (7) was confirmed by colony formation assays (Figure 1B). On the basis of these results, cells were either mock-irradiated or irradiated with 1 Gy of Fe ions or with 1 Gy (equal dose) or 4 Gy ('equal-survival' dose) of gamma rays. After ∼14 days of recovery, surviving cells were assayed *in vitro* as well as subcutaneously injected into nude mice. Metaphase chromosome spreads revealed that cells irradiated with Fe ions (but not those irradiated with gamma rays) exhibited a significant increase in Robertsonian fusions (50% of metaphase spreads, with an average of eight fusions per metaphase) (Figure 1C and D). These fusions, resulting from centromeric breakage by IR followed by fusion of two chromosomes at the breakage points, are a reliable indicator for the assessment of radiation-induced genomic instability (15). These data strongly suggest that inefficiently repaired DNA damage induced by Fe ions caused significantly more genomic instability compared with damage induced by gamma rays.

Ink4a/Arf−/− astrocytes irradiated with Fe ions are potently tumorigenic

We wanted to determine if some of the genomic changes wrought by Fe irradiation might have significant tumorigenic consequences and whether the degree of cellular transformation might be greater in magnitude after Fe exposure compared with gamma irradiation. Upon subcutaneous injection of surviving irradiated cells into nude mice, we found that mock-irradiated Ink4a/Arf−/− astrocytes consistently failed to generate tumors confirming their lack of tumorigenic potential (0/8 injections for mock–gamma irradiation and 0/8 injections for mock–Fe irradiation). Significantly, cells irradiated with Fe ions rapidly and consistently generated tumors 100% of the time (12/12) (Figure 2A). Cells irradiated with 1 Gy of gamma rays failed to form tumors (0/8), whereas those irradiated with a higher dose of 4 Gy formed tumors but only with a low frequency (2/8). The difference in frequency of tumor formation between Fe- and gamma-irradiated cells was determined to be statistically significant using Fisher's exact test (P value = 0.0007). A striking difference was also observed in the latency of tumor formation between Fe- and gamma-irradiated cells. On average, Fe-derived tumors first became palpable after 10.67 ± 2.7 days (mean ± SD), whereas the two gamma-derived tumors first

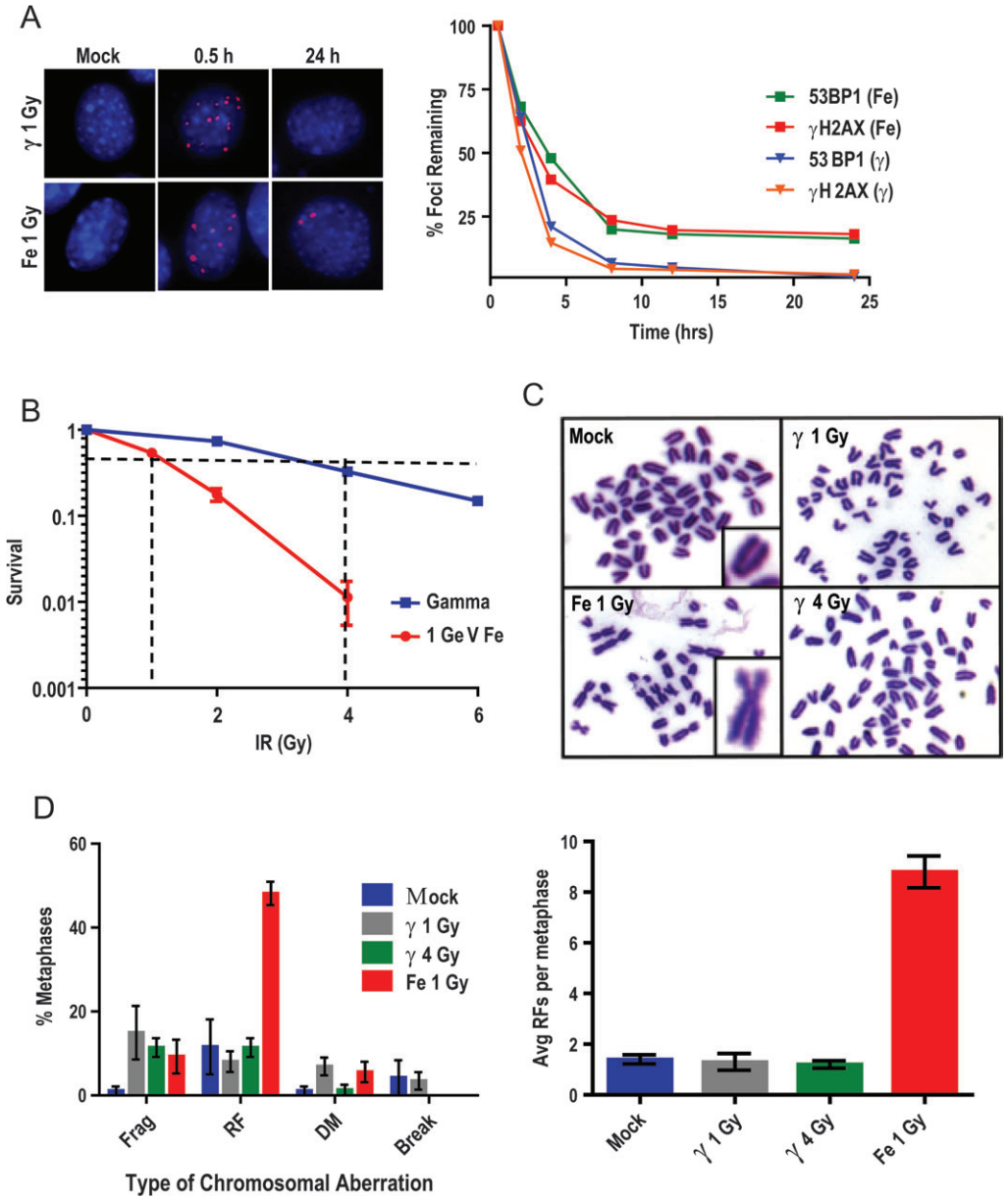

Fig. 1. DSBs induced by Fe ions are refractory to repair. (**A**) Primary Ink4a/Arf−/− astrocytes were irradiated with 1 Gy of gamma-rays or with 1 Gy of 1 GeV/nucleon Fe ions and coimmunostained with anti-γH2AX and anti-53BP1 antibodies. Initial damage (0.5 h) and residual damage (24 h) are depicted as γH2AX foci (red); nuclei are stained with 4′,6-diamidino-2-phenylindole (blue). γH2AX or 53BP1 foci were scored at different times postirradiation to obtain DSB repair kinetics. Percentage of foci remaining (*y*-axis) was plotted against repair time (*x*-axis). (**B**) Radiation survival was measured by colony formation assays. Fraction of surviving colonies (*y*-axis) was plotted against the corresponding radiation dose (*x*-axis). Dotted lines mark equal survival doses. (**C**) Metaphase chromosome spreads were prepared from mock- or gamma- or Fe-irradiated cells. Note increased frequency of Robertsonian fusions upon Fe irradiation (**D**) Frequency of chromosome aberrations (Frag, fragments; RF, Robertsonian fusions; DM, double minutes) was scored from metaphase spreads of mock- or gamma- or Fe-irradiated cells (average of 50 metaphases). Note significant increase in frequency of Robertsonian fusions in Fe-irradiated cells with an average of eight fusions per metaphase. Error bars represent standard error of the mean for all plots.

became palpable only after 46.5 ± 0.7 days. The difference in tumor growth curves for these two irradiation conditions was determined to be statistically significant using the generalized estimating equations method (P value = 0.001). Tumors derived from Fe-irradiated or gamma-irradiated cells stained positive for Ki67, pAkt and pErk, clearly indicating the activation of proproliferative pathways commonly upregulated in most cancers (16,17) (Figure 2B).

Ex vivo cultures of Fe-derived tumors exhibit rampant genomic instability

Ex vivo cultures of Fe-derived tumors displayed evidence of rampant genomic instability with high levels of Robertsonian fusions (100% of metaphase spreads and with an average of eight fusions per metaphase) and other gross chromosomal aberrations (such as double minutes and dicentric chromosomes) (Figure 2C). In order to identify the chromosomes participating in the Robertsonian fusions, we employed M-FISH staining, which allows simultaneous labeling of each mouse chromosome with a different color (18) (Figure 2D). M-FISH revealed that the Robertsonian fusions observed in Fe-derived tumor cells were random, involving almost all chromosomes (Figure 2E). These fusions were not seen at such high frequencies in the gamma-derived tumor cells, though very low frequencies of simple and reciprocal translocations were observed in these cells. In order to investigate telomere integrity, both at the chromosome ends as well as at the fusion points, we employed telomere fluorescence *in situ*

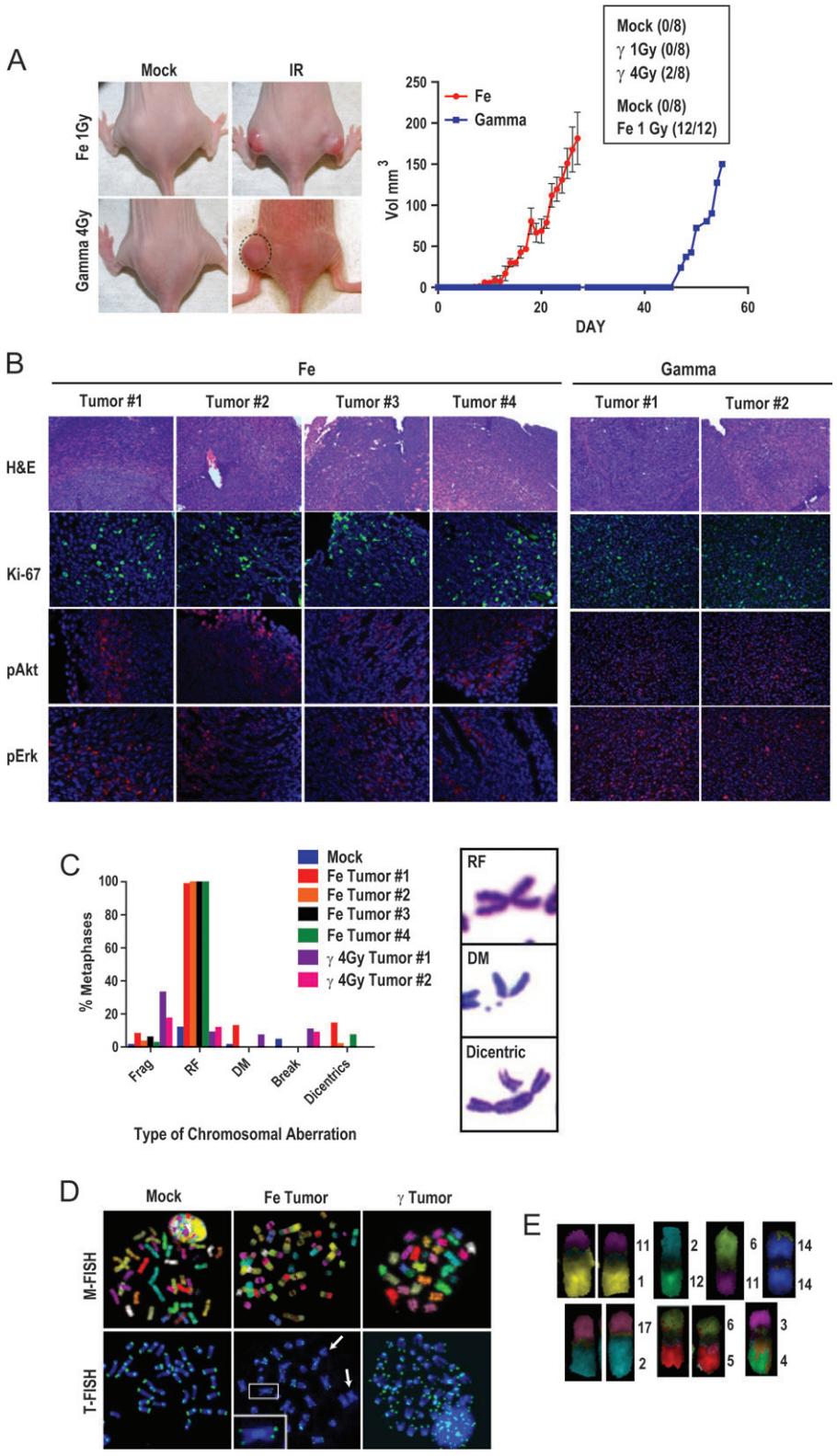

Fig. 2. Fe-irradiated Ink4a/Arf−/− astrocytes are potently tumorigenic. (**A**) Tumor development was monitored after subcutaneous injection of mock-gamma- or gamma- or mock-Fe- or Fe-irradiated astrocytes into nude mice. Representative pictures of tumor-bearing mice are shown (please note that only the left flank of 'Gamma 4 Gy' mouse shows tumor development; 'dashed circle'). Tumor volume (*y*-axis) was plotted against days postinoculation (*x*-axis). Tumor development frequencies are indicated as 'total tumors/total injections' ('box'). Differences in tumor frequency and growth were determined to be statistically significant using Fisher's exact test (*P* value = 0.0007) and generalized estimating equations method (*P* value = 0.001), respectively. Note rapid tumor development with Fe-irradiated astrocytes and slow and infrequent tumor formation with gamma-irradiated astrocytes. Error bars represent standard error of the mean. (**B**) Excised gamma-derived and Fe-derived tumors were sectioned and stained with hematoxylin and eosin or with the indicated antibodies. Nuclei are stained with 4′,6-diamidino-2-phenylindole (blue). (**C**) Frequency of chromosome aberrations (Frag, fragments; RF, Robertsonian fusions; DM, double minutes) observed in metaphase spreads from mock-irradiated or tumor-derived cells (average of 50 metaphases). Representative aberrations are shown. (**D**) For M-FISH, metaphase

hybridization staining, which specifically labels telomeric sequences (19). Telomere fluorescence *in situ* hybridization revealed the loss of telomeric signals, as expected (15), at the Robertsonian fusion points confirming that these fusions arose from centromeric breakage resulting in loss of telomeres at the short arms of acrocentric chromosomes (Figure 2D). Loss of telomeric signals was also observed at the ends of some chromosomes, only in the Fe-derived tumors, which would presumably perpetuate genomic instability through chromosome end-to-end fusions and repeated breakage–fusion–bridge cycles (20).

Fe-derived tumors exhibit common patterns of chromosomal copy number variation

Clearly, the Fe-derived tumor cells were significantly altered compared with mock-irradiated cells due to stochastic genomic changes induced by Fe ions, some of which, logically, were conducive to rapid tumor growth. Cells with such transforming genomic changes should have been selected for upon subcutaneous injection. We analyzed *ex vivo* cultures from Fe-derived tumors by array comparative genomic hybridization with the goal of identifying the common regions of deletion or amplification that would presumably harbor changes critical for tumorigenesis. Chromosomal copy number variation within the tumor isolates is shown, with green bars representing amplifications and red bars representing deletions (Figure 3A). Although both tumors had unique regions of deletion/amplification, there were also regions of copy number variation that were shared between the tumor samples and that might harbor genes important for particle-induced transformation: (i) a 13.9 Mb amplification of chromosome 2 (2qH1–qH3) harboring 160 genes, of which at least 17 are potential oncogenes; (ii) a 17.3 Mb amplification of chromosome 4 (4qD3–qE2) harboring 268 genes, of which 8 are potential oncogenes; (iii) a 190 kb deletion on chromosome 5 (5qA3) harboring a single gene with no reported role in tumor suppression; (iv) a 250 kb amplification of chromosome 8 (8qA2) harboring 4 genes, with no known oncogenes; (v) a 1.8 Mb amplification of chromosome 9 (9qA5.1) harboring 10 genes, with one potential oncogene; (vi) a 489 kb amplification of chromosome 17 (17qA1) harboring 6 genes, with no known oncogenes and (vii) a 276 kb deletion on chromosome 4 (4qC4–qC5) harboring 2 genes, both with critical tumor suppressor functions (see supplementary Table 1, available at *Carcinogenesis* Online, for table of potential oncogenes in the amplified regions, some of which could have presumably contributed to the transformation process).

Loss of p15/Ink4b is seen in tumors derived from Fe-irradiated Ink4a/Arf−/− astrocytes

Of these genomic alterations, we were particularly intrigued by the deleted region of chromosome 4 (4qC4–qC5) as there are only two

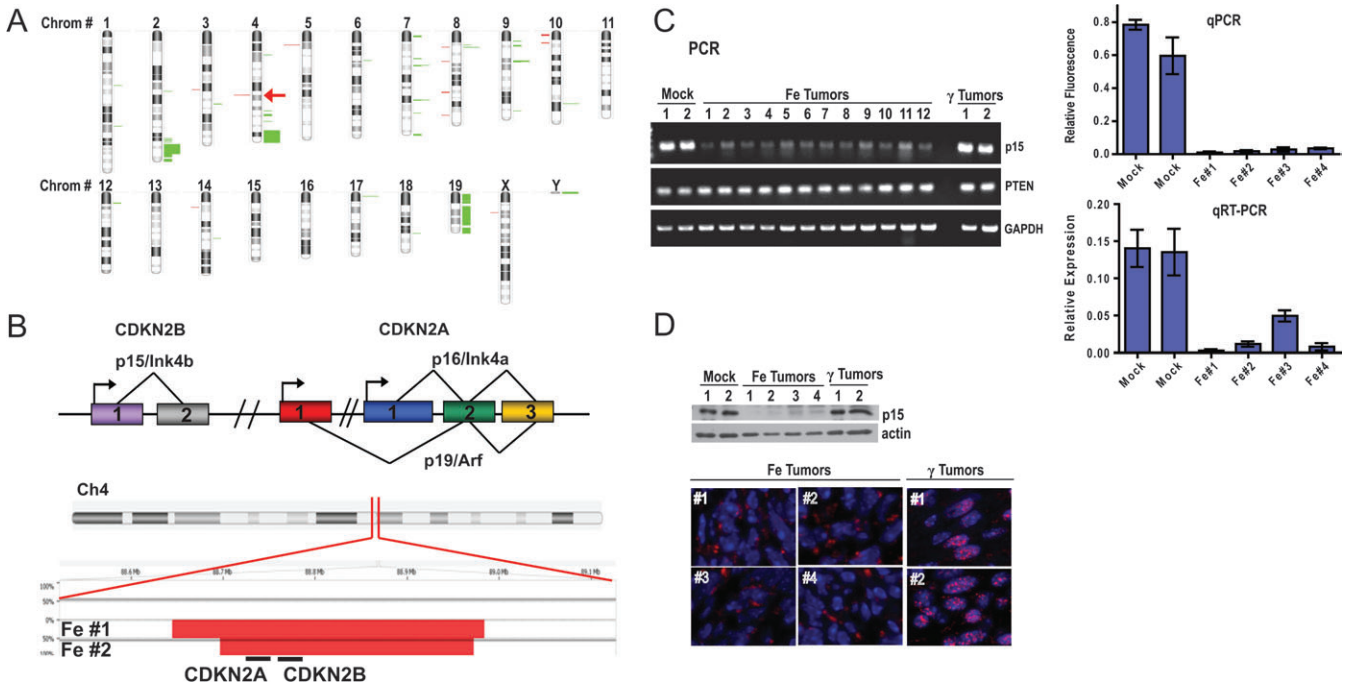

Fig. 3. Loss of p15/Ink4b in tumors derived from Fe-irradiated cells. (**A**) Chromosomal map of regions of copy number variation in Fe-derived tumor samples versus mock-irradiated cells derived by array comparative genomic hybridization and analyzed for DNA copy number changes using Nexus Copy Number Analysis software. The colored bands represent regions of amplification (green) or deletion (red) along each chromosome. The width of the band represents changes in either one or both samples. 'Red arrow' marks the *CDKN2A/CDKN2B* locus. (**B**) Schematic representation of the *CDKN2A/CDKN2B* genomic region, which encodes three tumor suppressors: p16/Ink4a, p19/Arf and p15/Ink4b. Map represents the deleted region of chromosome 4 for two tumor samples (derived by array comparative genomic hybridization and analyzed using Nexus software) showing the locations of *CDKN2A* and *CDKN2B* loci. (**C**) Loss of *p15/CDKN2B* locus was analyzed by PCR in 12 different *ex vivo* Fe-derived tumor cultures and the two gamma-derived tumor cultures; PCR analysis of the *PTEN* tumor suppressor locus was carried out for comparison. Loss of *p15/CDKN2B* locus was confirmed by quantitative PCR using genomic DNA from four different *ex vivo* tumor cultures. Loss of p15/Ink4b transcript was quantified by quantitative reverse transcription–PCR. Data were normalized to glyceraldehyde 3-phosphate dehydrogenase levels. Error bars represent standard error of the mean. (**D**) Loss of p15/Ink4b protein was analyzed by western blotting of whole-cells extracts from *ex vivo* tumor cultures and by staining tumor sections with anti-p15/Ink4b antibody. Note intense nuclear staining of p15/Ink4b in gamma-derived tumors and lack thereof in Fe-derived tumors.

spreads from mock-irradiated or tumor-derived cultures were hybridized with M-FISH probes comprising a cocktail of DNA labeling all mouse chromosomes. For telomere fluorescence *in situ* hybridization, metaphase spreads from mock-irradiated or tumor-derived cells were hybridized to a Cy3-peptide nucleic acid probe and counterstained with 4′,6-diamidino-2-phenylindole. Representative metaphase from Fe-derived tumor cells shows chromosomes with loss of telomeric signal at chromosome ends highlighted by 'arrows'. 'Inset' shows magnified image of a Robertsonian chromosome with loss of telomeric signal at the fusion point. (**E**) Representative M-FISH staining shows Robertsonian fusions occurring randomly between multiple chromosomes in Fe-derived tumors.

genes mapping to this region, *CDKN2A* and *CDKN2B* (Figure 3B) and our experiments involved irradiation of astrocytes derived from *CDKN2A* knockout mice (21). Clearly, deletion of the entire region must have provided the cells with an additional tumorigenic advantage over and above that conferred by the loss of *CDKN2A* alone. The only other gene in the deleted region, *CDKN2B*, codes for the p15/Ink4b tumor suppressor protein that has been reported to assume a greater role in tumor suppression in the absence of p16/Ink4a (12). We obtained evidence for loss of the *p15/Ink4b* locus in all 12 *ex vivo* tumor cultures by PCR and this was confirmed by qPCR analyses of four tumor-derived cultures (Figure 3C). Loss of p15/Ink4b transcript and protein was confirmed by quantitative reverse transcription–PCR (Figure 3C) and western analyses (Figure 3D), respectively, of four tumor-derived cultures. Immunofluorescent staining of four Fe-derived tumors showed major areas that were negative for p15/Ink4b staining (Figure 3D). Interestingly, the two gamma-derived tumors were positive for p15/Ink4b and exhibited intense nuclear staining for this protein (Figure 3D). Retention of p15/Ink4b in the gamma-derived tumors was confirmed by PCR and western analyses (Figure 3C and D). These results independently confirm the importance of p15/Ink4b in tumor suppression, especially in the absence of p16/Ink4a, and help explain why the entire *CDKN2A/CDKN2B* region is lost in many cancers (22–24). Given the striking differences in latency and frequency between high-LET Fe-derived tumors and low-LET gamma-derived tumors, it is tempting to speculate that loss of p15/Ink4b might contribute to the reduced latency and increased frequency of Fe-derived tumors.

Reexpression of p15/Ink4b results in inhibition of tumor growth

In order to investigate the possible effects of p15/Ink4b on tumor growth, we reexpressed V5-tagged human p15 in *ex vivo* cultures of Fe-derived p15-null tumors (Figure 4A). Tumor cells were transfected with pLenti6.3/p15-V5/DEST or with pLenti6.3/V5-GW/*lacZ* as a control. The Ink4 cell cycle inhibitors exert their functions by binding to the cyclin-dependent kinases, CDK4 and CDK6 (25). We first confirmed that the ectopically expressed p15 was functional and capable of binding both CDK4 and CDK6 by coimmunoprecipitation (Figure 4B). Tumor cells (control or p15-expressing) were then injected subcutaneously into nude mice and monitored for tumor formation. Although we did not observe a difference in tumor frequency, we observed a significant delay in the onset of tumor formation upon p15 reexpression (Figure 4C). On average, tumors generated from the control cells first became palpable after 6.58 ± 1.5 days (mean ± SD), whereas tumors from p15-expressing cells became palpable only after 19.17 ± 1.12 days. The difference in tumor growth curves was determined to be statistically significant using the generalized estimating equations method (P value = 0.008). Expression of p15 in tumors derived from p15-expressing cells was confirmed by immunofluorescence staining (Figure 4D). In sum, these results indicate that p15 loss may be a critical event in particle-induced tumorigenesis.

Discussion

In this study, we evaluated whether complex DSBs that are repaired slowly and incompletely (those induced by high-LET Fe ions) are more potently tumorigenic than simple breaks that can be repaired rapidly and completely (those induced by low-LET gamma rays). We hypothesized that Fe ions might generate a greater repertoire of genomic alterations compared with gamma rays that, in turn, might increase the likelihood of transforming genetic changes in the surviving cells. As wild-type cells usually harbor a number of fail-safe mechanisms to prevent tumorigenesis, we used 'sensitized' Ink4a/Arf−/− astrocytes (21) that might be rapidly transformed by IR, thus providing a simple yet sensitive paradigm for direct comparison of Fe ions with gamma

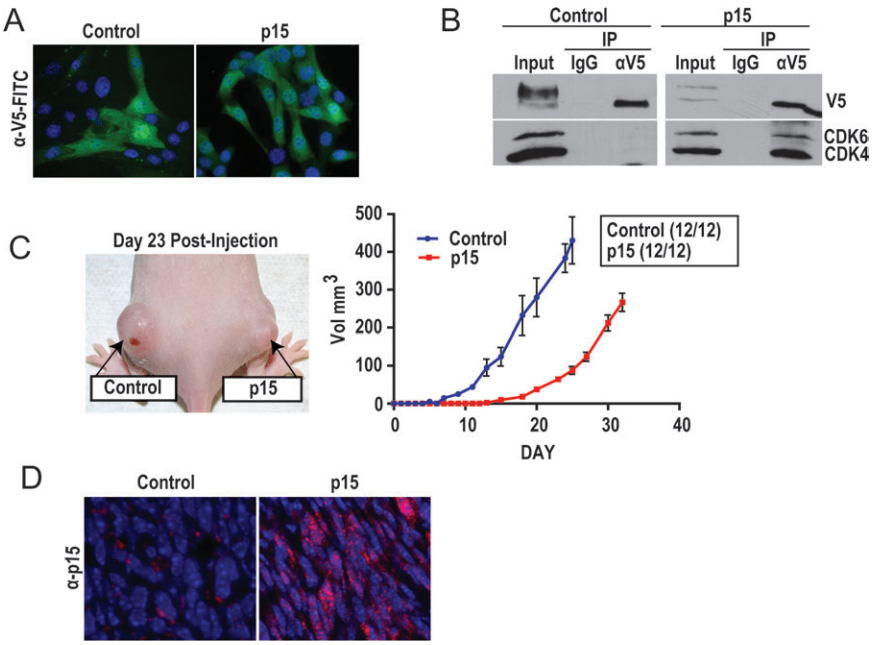

Fig. 4. Inhibition of tumor growth upon reexpression of p15/Ink4b. (**A**) *Ex vivo* cultures from Fe-derived p15-null tumors were transfected with a lentiviral vector expressing V5-tagged human p15 or the pLenti6.3/V5-GW/*lacZ* control vector. Immunofluorescent images of control and p15 reexpressing cells show positive staining with anti-V5-fluorescein isothiocyanate-conjugated antibody (green). Nuclei are stained with 4′,6-diamidino-2-phenylindole (blue). (**B**) Binding of ectopically expressed p15 to CDK4/6 was demonstrated by immunoprecipitating p15 with an anti-V5 antibody and western blotting the immunoprecipitates with anti-CDK4 and anti-CDK6 antibodies. Note coimmunoprecipitation of CDK4/6 from tumor cells reexpressing p15 but not from control tumor cells. (**C**) Tumor development was monitored after subcutaneous injection of control or p15-expressing tumor cells into nude mice. Representative picture of tumor-bearing mouse is shown. Note significant difference in tumor volume between control and p15-expressing tumors at 23 days postinjection. Tumor volume (y-axis) was plotted against days postinoculation (x-axis). Differences in tumor growth were determined to be statistically significant using the generalized estimating equations method (P value = 0.008). Tumor development frequencies show no difference and are indicated as 'total tumors/total injections' ('box'). (**D**) Excised tumors were sectioned and stained with anti-p15 antibody. Note positive p15 staining in tumors derived from p15-expressing cells and lack thereof in tumors derived from control cells.

rays. HZE particles are known to be more clastogenic than gamma rays (7), and a number of *in vitro* studies are testament to the transforming potential of these ions (26–30). Yet, very few studies have directly assessed the tumorigenic potential of these ions except for the mouse Harderian gland studies carried out at the Lawrence Berkeley and Oak Ridge National Laboratories (31,32); however, these studies did not analyze the genomic changes underlying tumor formation. In fact, genomic changes underlying IR-induced tumors are, in general, not well understood, except for radiation-induced thyroid cancers, where very specific gene rearrangements involving the *RET* (rearranged during transfection) proto-oncogene have been identified in humans (3) and for IR-induced medulloblastomas in *Ptch*+/− mice caused by loss of heterozygosity at the *Ptch* locus (33).

Our study is a careful analysis of genetic events that might play a causal role in particle-induced tumorigenesis. Using our model system, we show that Fe ions are potently tumorigenic compared with gamma rays and that the Fe-derived tumor cells are significantly genetically altered compared with the parental mock-irradiated cells. Copy number variation analyses of the Fe-derived tumor samples by array comparative genomic hybridization revealed common areas of amplifications and deletions. The amplified regions harbored a number of potential oncogenes (supplementary Table I is available at *Carcinogenesis* Online), some of which could have contributed to cellular transformation in our model system, and these will be analyzed in future studies. In this study, we focused on a small deletion in chromosome 4 resulting in loss of p15/Ink4b. Corresponding deletions in humans (in chromosome 9p21) are very common in many cancers including glioblastomas, which are tumors originating from astrocytes (22–24). The deleted region harbors the *CDKN2A* gene that codes for two very important tumor suppressors via alternate reading frames, Ink4a and Arf, which regulate the Rb and p53 tumor suppressor pathways, respectively (Figure 3b) (25). Deletion of this locus in our model system was particularly intriguing as this occurred in cells that were *CDKN2A*−/− to begin with, thereby indicating the importance of a second tumor suppressor gene in the deleted region, *CDKN2B*. In fact, it was first proposed by Bert Vogelstein that deletions in the 9p21 region are significantly more common than intragenic mutations in *CDKN2A* because of the presence of the neighboring gene *CDKN2B*, whose product (p15/Ink4b) might also play an important role in tumor suppression (34). Although the role of p16 as a 'bona fide' tumor suppressor is well documented, the importance of p15 in tumor suppression remains less well understood. Indeed, it was only recently demonstrated that p15 performs a critical backup function for p16 and that cells compensate for loss of p16 by increasing the levels of p15 protein under conditions of stress (12). Our results provide independent verification of the important tumor suppressor function of p15/Ink4b, especially in the context of p16/Ink4a loss, by demonstrating that (i) additional loss of p15/Ink4b upon Fe irradiation provides a tumorigenic advantage to cells already deficient in p16/Ink4a and (ii) reexpression of p15/Ink4b in tumor cells significantly delays tumor progression. The overall importance of the *CDKN2A/2B* locus is underscored by the following: (i) this locus is deleted in many cancers including gliomas (22–24), (ii) common variations (single nucleotide polymorphisms) in the *CDKN2A/2B* genes contribute to glioma susceptibility (35) and (iii) this locus is completely silenced in induced pluripotent stem cells and embryonic stem cells (36). Our results indicate that the *CDKN2A/2B* locus may be susceptible to deletion during particle-induced tumorigenesis, thereby bolstering the role of this locus as an important barrier to carcinogenesis.

Supplementary material

Supplementary Table 1 and References can be found at http://carcin.oxfordjournals.org/.

Funding

National Aeronautics and Space Administration (NNA05CS97G and NNX10AE08G to S.B.); Cancer Prevention and Research Institute of Texas (RP100644 to S.B.); Goldhirsh Foundation to R.M.B.; National Institutes of Health (CA122972 to D.A.B., CA129364 to C.S.N. and NS062080 to A.A.H.); National Cancer Institute (T32CA124334 to C.V.C.); U.S. Department of Energy (DE-FG02-05ER64055 to A.S.B.); National Aeronautics and Space Administration Specialized Center of Research (NNJ05HD36G); Flight Attendant Medical Research Institute (D.S.). This is CSCN 050.

Acknowledgements

Conflict of Interest Statement: None declared.

References

1. Little,J.B. (2000) Radiation carcinogenesis. *Carcinogenesis*, **21**, 397–404.
2. Wakeford,R. (2004) The cancer epidemiology of radiation. *Oncogene*, **23**, 6404–6428.
3. Volpato,C.B. *et al*. (2008) Enhanced sensitivity of the RET proto-oncogene to ionizing radiation in vitro. *Cancer Res.*, **68**, 8986–8992.
4. Hamatani,K. *et al*. (2008) RET/PTC rearrangements preferentially occurred in papillary thyroid cancer among atomic bomb survivors exposed to high radiation dose. *Cancer Res.*, **68**, 7176–7182.
5. O'Driscoll,M. *et al*. (2006) The role of double-strand break repair—insights from human genetics. *Nat. Rev. Genet.*, **7**, 45–54.
6. Hada,M. *et al*. (2006) Spectrum of complex DNA damages depends on the incident radiation. *Radiat. Res.*, **165**, 223–230.
7. Durante,M. *et al*. (2008) Heavy ion carcinogenesis and human space exploration. *Nat. Rev. Cancer*, **8**, 465–472.
8. Cucinotta,F.A. *et al*. (2006) Cancer risk from exposure to galactic cosmic rays: implications for space exploration by human beings. *Lancet Oncol.*, **7**, 431–435.
9. Schulz-Ertner,D. *et al*. (2007) Particle radiation therapy using proton and heavier ion beams. *J. Clin. Oncol.*, **25**, 953–964.
10. Mukherjee,B. *et al*. (2008) Modulation of the DNA-damage response to HZE particles by shielding. *DNA Repair (Amst.)*, **7**, 1717–1730.
11. Bachoo,R.M. *et al*. (2002) Epidermal growth factor receptor and Ink4a/Arf: convergent mechanisms governing terminal differentiation and transformation along the neural stem cell to astrocyte axis. *Cancer Cell*, **1**, 269–277.
12. Krimpenfort,P. *et al*. (2007) p15Ink4b is a critical tumour suppressor in the absence of p16Ink4a. *Nature*, **448**, 943–946.
13. Mukherjee,B. *et al*. (2009) EGFRvIII and DNA double-strand break repair: a molecular mechanism for radioresistance in glioblastoma. *Cancer Res.*, **69**, 4252–4259.
14. Zijlmans,J.M. *et al*. (1997) Telomeres in the mouse have large inter-chromosomal variations in the number of T2AG3 repeats. *Proc. Natl Acad. Sci. USA*, **94**, 7423–7428.
15. Boei,J.J. *et al*. (1996) Classification of X-ray-induced Robertsonian fusion-like configurations in mouse splenocytes. *Int. J. Radiat. Biol.*, **69**, 421–427.
16. Altomare,D.A. *et al*. (2005) Perturbations of the AKT signaling pathway in human cancer. *Oncogene*, **24**, 7455–7464.
17. Roberts,P.J. *et al*. (2007) Targeting the Raf-MEK-ERK mitogen-activated protein kinase cascade for the treatment of cancer. *Oncogene*, **26**, 3291–3310.
18. Bayani,J. *et al*. (2004) Multi-color FISH techniques. *Curr. Protoc. Cell Biol.,* Chapter 22, Unit 22 5.
19. Scherthan,H. (2002) Detection of chromosome ends by telomere FISH. *Methods Mol. Biol.*, **191**, 13–31.
20. Murnane,J.P. (2006) Telomeres and chromosome instability. *DNA Repair (Amst.)*, **5**, 1082–1092.
21. Serrano,M. *et al*. (1996) Role of the INK4a locus in tumor suppression and cell mortality. *Cell*, **85**, 27–37.
22. Cannon-Albright,L.A. *et al*. (1992) Assignment of a locus for familial melanoma, MLM, to chromosome 9p13-p22. *Science*, **258**, 1148–1152.
23. Lukas,J. *et al*. (1995) Retinoblastoma-protein-dependent cell-cycle inhibition by the tumour suppressor p16. *Nature*, **375**, 503–506.
24. Nobori,T. *et al*. (1994) Deletions of the cyclin-dependent kinase-4 inhibitor gene in multiple human cancers. *Nature*, **368**, 753–756.
25. Kim,W.Y. *et al*. (2006) The regulation of INK4/ARF in cancer and aging. *Cell*, **127**, 265–275.
26. Borek,C. *et al*. (1978) Malignant transformation in cultured hamster embryo cells produced by X-rays, 460-keV monoenergetic neutrons, and heavy ions. *Cancer Res.*, **38**, 2997–3005.

27. Hei,T.K. *et al*. (2001) Molecular alterations in tumorigenic human bronchial and breast epithelial cells induced by high LET radiation. *Adv. Space Res.*, **27**, 411–419.
28. Li,H. *et al*. (2007) Malignant transformation of human benign prostate epithelial cells by high linear energy transfer alpha-particles. *Int. J. Oncol.*, **31**, 537–544.
29. Yang,T.C. *et al*. (1997) Initiation of oncogenic transformation in human mammary epithelial cells by charged particles. *Radiat. Oncol. Investig.*, **5**, 134–138.
30. Zhao,Y. *et al*. (2004) Down-regulation of Betaig-h3 gene is involved in the tumorigenesis in human bronchial epithelial cells induced by heavy-ion radiation. *Radiat. Res.*, **162**, 655–659.
31. Alpen,E.L. *et al*. (1993) Tumorigenic potential of high-Z, high-LET charged-particle radiations. *Radiat. Res.*, **136**, 382–391.
32. Fry,R.J. *et al*. (1985) High-LET radiation carcinogenesis. *Radiat. Res. Suppl.*, **8**, S188–S95.
33. Pazzaglia,S. *et al*. (2006) Linking DNA damage to medulloblastoma tumorigenesis in patched heterozygous knockout mice. *Oncogene*, **25**, 1165–1173.
34. Jen,J. *et al*. (1994) Deletion of p16 and p15 genes in brain tumors. *Cancer Res.*, **54**, 6353–6358.
35. Shete,S. *et al*. (2009) Genome-wide association study identifies five susceptibility loci for glioma. *Nat. Genet.*, **41**, 899–904.
36. Li,H. *et al*. (2009) The Ink4/Arf locus is a barrier for iPS cell reprogramming. *Nature*, **460**, 1136–1139.

Received March 16, 2010; revised July 2, 2010; accepted July 19, 2010